Title

Destruction of the Uranyl Moiety in a U(V) “Cation—Cation” Interaction

Journal

Inorganic Chemistry, 58(15)

ISSN

0020-1669

Authors

Hu, Shu-Xian

Jian, Jiwen

Li, Jun

et al.

Publication Date

2019-08-05

DOI

10.1021/acs.inorgchem.9b01265

Peer reviewed

Destruction of the uranyl moiety in a U(V) "cation-cation" interaction

Shu-Xian Hu,[a,b] Jiwen Jian,[c,‡] Jun Li, [b,d*] John K. Gibson[c,*]

[a] *Beijing Computational Science Research Center, Beijing 100193, China*

[b] *Department of Chemistry and Key Laboratory of Organic Optoelectronics & Molecular Engineering of Ministry of Education, Tsinghua University, Beijing 100084, China*

[c] *Chemical Sciences Division, Lawrence Berkeley National Laboratory, Berkeley, California 94720, USA*

[d] *Department of Chemistry, Southern University of Science and Technology, Shenzhen 518055, China*

[‡]Current address: Hangzhou Institute of Advanced Studies, Zhejiang Normal University, 1108 Gengwen Road, Hangzhou, Zhejiang, 311231, China

[*]Corresponding authors email addresses:
junli@tsinghua.edu.cn (Li); jkgibson@lbl.gov (Gibson)

Abstract

A gas-phase uranyl peroxide dimer supported by three 12-Crown-4 ether (12C4) ligands, $[(UO_2)_2(O_2)(12C4)_3)]^{2+}$ (**A**), was prepared by electrospray ionization. Density functional theory (DFT) indicates a structure with two terminal 12C4 and the third 12C4 bridging the uranium centers. Collision induced dissociation (CID) of **A** resulted in elimination of the bridging 12C4 to yield a uranyl peroxide dimer with two terminal donor ligands, $[(12C4)(UO_2)(O_2)(UO_2)(12C4)]^{2+}$ (**B**). Remarkably, CID of **B** resulted in elimination of the bridging peroxide concomitant with reduction of U(VI) to U(V) in **C**, $[(12C4)(UO_2)(UO_2)(12C4)]^{2+}$. DFT indicates that in **C** there is direct interaction between the two UO_2^+, which can thus be considered as a so-called cation-cation interaction (CCI). This formal CCI, induced by tetradentate 12C4 ligands, corresponds to destruction of the linear uranyl moieties and creation of bridging U-O-U oxo-bonds. Based on the structural rearrangement to achieve the structurally extreme CCI interaction, it is predicted to also be accessible for PaO_2^+, but is less feasible for transuranic actinyls.

Keywords: Cation-cation interaction • Uranium(V) • Uranyl peroxide • Uranium coordination complex

Introduction

The chemistry of the pentavalent uranyl ion, UO_2^+ or simply U(V), is important for understanding the behavior of uranium in the environment, wastes, and spent nuclear fuel processing.[1-2] Under most environmental and process conditions U(V) is unstable relative to U(IV) and U(VI),[1, 3-4] but U(V) can be stabilized in the absence of other redox agents, and is furthermore intermediate in U redox processes such as photocatalysis,[5] and photochemical and microbiological reduction of U(VI).[6]

Coordination of actinide ions by multicoordinate ligands has attracted attention as a route to unique molecular structures, and for possible utility in environmental and nuclear waste management.[7-8] Uranyl, $UO_2^{+/2+}$,[2, 9-10] has received particular attention due to its environmental abundance, and as a model for heavier actinides. Ligand attributes that might be adjusted for more efficient and controlled actinide complexation and separations include provision of multi-functionalized electron-donor sites, variable chelate ring size, and ligand preorganization.[11-13] Beyond potential utility in advanced separations and other technologies, fundamental exploration of actinide complexation has largely focused on bonding, and on structural and electronic effects. Among the many type of designed ligands, multicoordinate macrocyclic O-donors have exhibited particularly enhanced separation efficiencies.[8] Crown ethers are model multidentate O-donor ligands that can selectively bind metal ions, usually due to a size match between the crown cavity and cation.[14] As a result, crown ethers have potential for actinide partitioning from nuclear waste,[15-16] particularly via size-specificity.[17-20] Gas-phase actinide crown ether complexes, including of uranyl, present a means to elucidate factors that affect complexation and coordination, including geometric effects that may be supported by distinctive crown geometries.[18, 20] In the present work we extend this general line of inquiry from mononuclear uranyl-crown complexes to dimeric uranyl complexes, with an aim to understand how crown ethers might act as bridging ligands and support novel bonding motifs such as cation-cation interactions. Studied here is the smallest simple crown ether, 12-Crown-4 denoted hereafter as 12C4.

The UO_2^+ cation, and other actinyl(V) and actinyl(VI) cations, can coordinate other cations via their electron-donor O atoms,[3, 21-22] a phenomenon commonly dubbed a cation-cation interaction (CCI).[23-26] In a CCI between two actinyl cations the interionic Coulomb repulsion is offset by attraction between a negatively charged oxygen atom of one actinyl and the positively charged actinide center of the other. Although a more elaborate and accurate description of this type of interaction might be as an "extreme dipole interaction between cationic molecules", we retain the convenient conventional terminology of "CCI", where the quotation marks, as employed by Guillaume et al.,[27] emphasize that the attractive interaction is an actinide-oxygen dipole interaction, not an interaction between bare atomic cations. CCIs between actinyls are feasible because the net positive charge on the actinyl provides an exaggerated charge on the actinide metal center, while still retaining a significant negative charge on the oxygen atoms.[28] Because of their potential role in crystal chemistry,[29] and in solution chemistry of penta- and hexavalent uranium,[30] CCIs have received considerable attention,[31-32] including for purported function in disproportionation of U(V).[33-34] The uranyl(VI) peroxide dimer, first reported by Burns et al. in 2005, acts as a building block for nanostructures;[35-36] in the

$[(UO_2)(O_2)(UO_2)]^{2+}$ dimeric unit, the U(VI) moieties are linked by bridging peroxide.[37-39] A potential, but as yet unreported, phenomenon of interest in the context of the present work is formation of a U(V)-U(V) CCI from direct reduction of U(VI)-U(VI) dimeric moieties such as those reported by Burns et al.

A central goal of gas-phase chemistry is to investigate phenomena like actinyl CCIs at elementary and fundamental levels, with overarching objectives of enhanced understanding and, ideally, better control of chemistry in pragmatic scenarios. To explore CCIs in gas phase, we adopt a very simple notion derived from early reports of solution CCIs by Sullivan and co-workers as "a specific interaction between the oxygenated cations Np(V) and U(VI)".[40] In this vein, a U(V)-U(V) CCI can be considered as a specific interaction between two UO_2^+ moieties. An attribute of a uranyl CCI that derives from solution behavior, and differentiates CCIs from other types of uranyl dimers, is a direct unmediated bonding interaction between two $U^VO_2^+$ and/or $U^{VI}O_2^{2+}$ moieties. This attribute is not fulfilled, for example, in a ligand (L) supported peroxide dimer $[(L)(UO_2)(O_2)(UO_2)(L)]^{2+}$, where the bridging peroxide interposed between the uranyl(VI) moieties drastically moderates the U(VI)-U(VI) interaction. The key CCI attribute would be fulfilled in dimer $[(L)(UO_2)(UO_2)(L)]^{2+}$, where the bridging peroxide has been eliminated.

General types of actinyl CCIs are illustrated in Scheme 1. Even the extreme of essentially bridging oxygen atoms in structure (d) can reasonably be considered as a CCI because the interacting moieties are two UO_2^+ with no intervening peroxide or other moiety. Furthermore, cleavage of CCI dimer (d) in Scheme 1 would result in two mononuclear uranyl(V), UO_2^+. According to this classification, a CCI is characterized by the general nature of the cation-cation interaction, rather than by retention of two intact uranyl moieties. As is the case for a solution CCI, a gas-phase CCI can be facilitated by secondary coordinating ligands that serve to stabilize the overall system. It is the direct (UO_2^+)-(UO_2^+) interaction in all four scenarios in Scheme 1 that is the key attribute of a CCI. The significance of potential structurally extreme CCIs such as structure (d) in Scheme 1 derives from interest in understanding how to generally create and control such distinctive bonding motifs—conventional CCIs such as structures (a) and (b) should be elucidated by structures such as (c) and (d) that involve progressively more extreme distortions of the actinyl subunits. It should be remarked that structures (a) to (d) are shown for illustration, and there is actually a continuum of CCIs between these extremes, which is an appealing aspect of probing to the extent possible across the entire range of CCIs.

We here report gas-phase complexes of uranyl peroxide dimers with various degrees of coordination by 12C4 ligands, and also a novel $[UO_2^+ \cdot UO_2^+]$ CCI. The starting complex $[(UO_2)(O_2)(UO_2)(12C4)_3]^{2+}$ was prepared by electrospray ionization (ESI), and derivative ions were then prepared by collision induced dissociation (CID). The CID products are not coordinatively saturated and thus exhibit spontaneous water addition. Density functional theory (DFT) and *ab initio* wavefunction methods provide geometric parameters and bonding properties, including evidence for a uranyl(VI) peroxide dimer coordinated by three 12C4, and an extreme uranyl(V) CCI formed by elimination of the bridging peroxide unit.

Experimental Methods

The formation of gas-phase uranyl-12C4 complexes by ESI and CID, and their water-addition chemistry, was studied using an Agilent 6340 quadrupole ion trap mass spectrometer (QIT/MS).[41] The general approach has been described elsewhere, including for studies of hydration of uranyl-crown complexes.[42] $[(UO_2)(O_2)(UO_2)(12C4)_3]^{2+}$ was produced by ESI of a solution of ~100 μM uranyl chloride and ~400 μM 12C4 (Sigma-Aldrich ⩾98%) in moist ethanol (<10% water). Ions were isolated and subjected to CID, whereby they are excited and undergo multiple energetic collisions with helium to induce dissociation. The applied CID voltage is an instrumental parameter that does not provide an absolute excitation energy, but higher voltage does indicate greater relative energy. As discussed elsewhere, the background H_2O and O_2 pressures in the ion trap are estimated to be on the order of 10^{-6} Torr, while the helium buffer gas pressure is $\sim 10^{-4}$ Torr.[41] Other reagent gases such as acetonitrile can be introduced into the ion trap at pressures comparable to that of background gases. Mass spectra were acquired using the following instrumental parameters: solution flow rate, 60 μL min^{-1}; nebulizer gas pressure, 15 psi; capillary voltage, -3500 V; end plate voltage offset, −500 V; dry gas flow rate, 5 L/min; dry gas temperature, 325 °C; capillary exit, 132.6 V; skimmer, 40.0 V; octopole 1 and 2 dc, 12.0 and 1.70 V; octopole RF amplitude, 195.0 Vpp; lens 1 and 2, −5.0 and −60.0 V; trap drive, 62.3. High-purity N_2 for nebulization and drying was boil off vapor from a liquid nitrogen Dewar.

Computational Methods

Quantum chemical calculations were performed at the level of DFT with scalar relativistic corrections using computational chemistry software packages Gaussian 09[43] and ADF 2016.[44-45] In initial searching for the most stable isomer, the generalized gradient approximation (GGA) with the PBE functional was used.[46] To balance between accuracy and time cost of the calculations, in ADF we applied the frozen core approximation for $[1s^2\text{-}5d^{10}]$ of the U atom, and for C and O atoms a frozen $[1s^2]$ shell and Slater-type basis sets of valence triple-zeta plus two polarization functions (TZ2P) quality.[47-48] Relativistic effects were accounted for using the scalar relativistic (SR) zero-order-regular approximation (ZORA).[49] Owing to small polarizability and strong correlation of the inner contracted U(5f) shell, geometry optimizations and vibrational frequency analyses were further performed with B3LYP[50-51] hybrid density functional using Gaussian 09. The scalar-relativistic Stuttgart energy-consistent pseudopotential with 32-valence-electrons and the associated ECP60MWB_SEG valence basis set[52] were used for U, and Dunning's correlation consistent all-electron basis sets with polarized triple-zeta (cc-pVTZ)[53] were used for O, C and H. This methodology has been successfully applied to other actinide systems.[17] Geometry optimizations were performed without symmetry restrictions and were followed by vibrational frequency analysis to assign optimized structures as local minima or saddle points. Reaction energies were obtained by combining electronic energies with zero-point vibrational energy corrections. Scaling of coupled cluster methods including dynamic electron correlation, DLPNO-CCSD(T) with DKH-def2-TZVP(U): def2-SVP(C,H,O) basis sets were

performed using the Orca 4.01 program.[54] These single-point calculations were performed on the optimized B3LYP geometries. The relative energies confirmed essential results from B3LYP, with reasonable energy deviations for different methods and basis sets.[55]

In further electronic structure calculations on the B3LYP optimized structures, the B3LYP functional with ADF was used in conjunction with Slater type orbitals (STOs) of the quality of triple-zeta plus two polarization functions (TZ2P). Energy decomposition analyses (EDA) and combined Extended Transition State with the Natural Orbitals for Chemical Valence (EDA-NOCV) theory were used to assess orbital contributions to total bonding energies.[56-59] Electron localization functions (ELF)[60] were determined based on the PBE results from ADF. Bond order analyses were performed based on the Mayer method (BO_{Mayer}),[61] the Gopinathan-Jug indices (BO_{GJ})[62], and the Nalewajski-Mrozek method (BO_{NM})[56, 63]. Charge analyses are based on Mulliken method,[64] Hirshfeld analysis,[65] Voronoi deformation density,[66] and Multipole derived charges (MDC)[67]. The Weinhold's natural bond orbitals (NBO)[68] and natural localized molecular orbitals (NLMOs)[69] analyses were performed at the B3LYP/6-31g level using the NBO 6.0 program.[70] In all calculations there was no evaluation of effects of spin-orbit coupling, which is not expected to substantially affect the essential conclusions.

Results and Discussion

ESI and CID Synthesis of Uranyl-12C4 Dimer Complexes

The mass spectrum obtained for ESI of a solution of UO_2Cl_2:12C4 (1:4 in ethanol / <10% water) was reported previously[20] and is shown in Figure S1. The previous focus was on complexes of one uranyl coordinated by 12C4. The peak at 550 m/z corresponds to dimer $[(UO_2)(O_2)(UO_2)(12C4)_3]^{2+}$, denoted **A**; the composition and charge of **A** was confirmed by CID described below. We initially presumed that **A** consists of two uranyl moieties linked by a bridging peroxide, in analogy with previously reported [(DMA)-(UO_2)-(O_2)-(UO_2)-(DMA)]$^{2+}$ where terminal donor ligands DMA are 2,2′-trifluoroethylazanediyl-bis-N,N′-dimethylactamide.[71] We tentatively postulate that $[(12C4)(UO_2)(O_2)(UO_2)(12C4)]^{2+}$ should correspond to replacement of the terminal DMA by 12C4, which begs consideration as to the disposition of the third 12C4 ligand in **A**. If two terminal 12C4 coordinate to uranyls linked by a peroxide, what is the situation of the "extra" 12C4? Does it somehow bridge and bind to both uranyls? The appearance of seemingly peculiar **A** motivated the integrated experiment and theory inquiry reported here.

The mass spectrum obtained for CID of **A**, shown in Figure 1, reveals dominant dipositive products $[(UO_2)_2(O_2)(12C4)_2]^{2+}$, denoted as **B**, and $[(UO_2)_2(12C4)_2]^{2+}$, denoted as **C**. That **B** is intermediate from **A** to **C** was confirmed by secondary CID of **B**, which yielded primarily **C**, as shown in Figure 2. The two key reactions inferred from the CID results are thus (1) and (2).

$[(UO_2)_2(O_2)(12C4)_3]^{2+}$ (**A**) → $[(UO_2)_2(O_2)(12C4)_2]^{2+}$ (**B**) + 12C4 (1)

$[(UO_2)_2(O_2)(12C4)_2]^{2+}$ (**B**) → $[(UO_2)_2(12C4)_2]^{2+}$ (**C**) + O_2 (2)

Spontaneous Water Addition to B and C

Adventitious background gases in the ion trap include H_2O and O_2, both of which can potentially react with cations such as uranyl.[41] Addition of H_2O to a generic metal oxide cation XO^{n+} (n = 1 or 2) can proceed by non-dissociative physisorption to yield a hydrate, $XO^{n+}\cdot(H_2O)$, or dissociative chemisorption to yield a hydroxide, $X(OH)_2^{n+}$. Water addition to dipositive cations like **B** and **C** results in the appearance of peaks at +9 m/z in CID spectra, such as in Figures 1 and 2. The peaks identified at +18 m/z could result from addition of two H_2O to dipositive **B** or **C**, or addition of one water to monopositive ions having the same m/z. In particular, $[(UO_2)(O)(12C4)]^+$ has the same m/z as **B**, and $[(UO_2)(12C4)]^+$ the same m/z as **C**. The CID spectra in Figures 2 and 3 reveal water addition, with Δ(m/z) = +9 indicating dipositive **B** and **C**.

Water-addition reactions of **B** and **C** were studied in more detail by isolating ions with appropriate m/z, followed by applying reaction time t_{ap} that is the additional time after the fixed intrinsic ion isolation period of ~0.05 s. In contrast to energetic CID, these conditions correspond to an ion-molecule reaction temperature of ~300 K,[72] such that bimolecular reactions must be exothermic (or thermoneutral) and not have kinetic barriers above the reactant energy asymptote.

Based on the following considerations, the reaction results in Figure 3 demonstrate that species at 462 m/z is predominantly dipositive **B**, possibly with some contribution from monopositive $[(UO_2)(O)(12C4)]^+$. Whereas peak ***a*** at Δ(m/z) = +9 must be due to addition of an H_2O molecule to **B**, ***b*** at Δ(m/z) = +18 could be due to addition of two H_2O to **B** and/or one H_2O to $[(UO_2)(O)(12C4)]^+$. The time evolution of peak intensities reveals ***b*** as predominantly from **B**. Specifically, increasing t_{ap} from 0 s to 0.1 s resulted in minor change in the relative intensity of peak ***a*** but a significant increase in ***b***. If both ***a*** and ***b*** were due to addition of one water, to **B** and $[(UO_2)(O)(12C4)]^+$ respectively, the intensities of both should increase in parallel. Instead, near invariance of ***a*** concomitant with increasingly abundant ***b*** indicates addition of two H_2O, to yield sequentially ***a*** and then ***b***. A minor contribution from $[(UO_2)(O)(12C4)]^+$ cannot be excluded.

The results in Figure 4 provide an assessment of contributions from dipositive **C** and monopositive $[(UO_2)(12C4)]^+$, both 446 m/z. The appearance of peak ***c*** Δ(m/z) = +9 indicates **C**; abundant ***d*** suggests a significant contribution from water-addition to $[(UO_2)(12C4)]^+$. At the longer reaction time (t_{ap} = 0.1 s), additional product ***e*** indicates O_2 addition to monopositive $[(UO_2)(12C4)]^+$; ***f*** corresponds to addition of H_2O to ***e***. From previous results,[41, 73] we suppose that addition of O_2 to $[(UO_2)(12C4)]^+$ yields a U(VI) superoxide. Reaction of **C** with acetonitrile in the ion trap (Figure S3) suggest sequential addition of two CH_3CN to **C**, with a contribution from $[(UO_2)(12C4)]^+$. The aggregate results in Figures 4 and S3 indicate that the peak at 446 m/z is a mixture of **C** and $[(UO_2)(12C4)]^+$.

The above results demonstrate that **B** and **C** spontaneously and exothermically react with water to sequentially associate with H_2O, reactions (3)-(6); (6) is not definitively established due to a significant contribution from $[(UO_2)(12C4)]^+$. Reactions (3)-(6) do not reveal whether the process is physisorption to yield a hydrate or chemisorption to yield a hydroxide. Reactivity with acetonitrile, Figures S3 and S5, reveals that **B** and **C** similarly add acetonitrile. Because dissociation of CH_3CN is not feasible in these experiments, the products are assigned as physisorption adducts. The acetonitrile results do not

definitively illuminate water association because dissociation of water is more accessible. To further address the nature of the dimers we turn to quantum electronic structure calculations.

B + H_2O → **B**.H_2O (3)

B.H_2O + H_2O → **B**.2H_2O (4)

C + H_2O → **C**.H_2O (5)

C.H_2O + H_2O → **C**.2H_2O (6)

Structure of $[(UO_2)_2(O_2)(12C4)_3]^{2+}$ (A): 12C4 Ligands as Both Terminal and Bridging

As geometries optimized with density functionals PBE and B3LYP are similar, only the latter are presented. Single-point energies of the most stable structures were determined at the *ab initio* DLPNO-CCSD(T) level using optimized B3LYP geometries. Reaction energies are in Table 1; formation energies for the lowest energy structures are in Table 2. Geometric parameters for **A**, **B** and **C** and hydrates are in Table 3; B3LYP structures and energies of ground-state (GS) species are detailed in SI. GS structures for **A**, **B** and **C** are shown in Figure 5. In the following discussion we identify oxygen atoms as: O_L = 12C4 ligand-based; O_{yl} = uranyl (O_{yl}=U=O_{yl}); O_b = bridging (U-O_b-U); O_t = terminal (U=O_t); O_w = water (H_2O_w···U).

Low-energy structures and energies of $[(UO_2)_2(O_2)(12C4)_3]^{2+}$ are shown in SI Tables S2 and S3. $[(UO_2)_2(O_2)(12C4)_3]^{2+}$ GS isomer **A**, also in Figure 5, is characterized by a $[(UO_2)(O_2)(UO_2)]^{2+}$ core coordinated by three 12C4. The energy for association of $[(UO_2)(O_2)(UO_2)]^{2+}$ with two 12C4 is -231 kcal/mol (Table 2, B3LYP). The reported structure for $[UO_2(12C4)_2]^{2+}$ has side-on equatorial coordination of U by six O_L. In contrast, $[(UO_2)_2(O_2)(12C4)_3]^{2+}$ has both U penta-coordinated in the quasi-equatorial plane, by three O_L from 12C4 and two O_b from the bridging peroxide. Two 12C4 exhibit bidentate coordination with U-O_L distances of ~2.5 Å, with other U-O_L distances >3.9 Å. The third 12C4 binds side-on in the equatorial uranyl plane with an O_L coordinating to both U with U-O_L distances of ~2.5 Å. The structure of **A** in Figure 5 is characterized by two "bridges" between the uranyl centers: the peroxide moiety forms a typical "direct" bridge between the two U; the 12C4 bridge is more distinctive in forming a "London Bridge" structure, as an oxygen-anchored tower that links the two U.

In contrast to bare $[(UO_2)(O_2)(UO_2)]^{2+}$ (Table 3), this same moiety embedded in **A** has a non-planar structure with a U1-(O_bO_b)-U2 dihedral angle of ca. 49°, where this angle is that defined by the two U atoms and the two O_b atoms (0° would be planar). As a result of coordination of the uranyl moieties in **A** the U-O_{yl} bond lengths are elongated relative to the bare dimer, from ~1.72 to ~1.76 Å. The $O_{yl}UO_{yl}$ angle is ~172° in $[(UO_2)(O_2)(UO_2)]^{2+}$ and ~174° in **A**. Due to ligand charge donation,[74] the uranyl ν_1 symmetric stretch mode of **A** is red-shifted to 981 cm^{-1}, from 1063 cm^{-1} for unligated $[(UO_2)(O_2)(UO_2)]^{2+}$.

Structure of $[(UO_2)_2(O_2)(12C4)_2]^{2+}$ (B): A "Conventional" Uranyl Peroxide Dimer

CID of $[(UO_2)_2(O_2)(12C4)_3]^{2+}$ (**A**) resulted in $[(UO_2)_2(O_2)(12C4)_2]^{2+}$ (**B**). Elimination of one 12C4

from **A** to yield **B**, CID reaction (1), requires 57 kcal/mol. The GS structure of **B** in C_2 symmetry, shown in Figure 5, has a central uranyl peroxide dimer as in **A**, with terminal tetradentate 12C4 ligands and U-O_L bond distances of 2.7-2.9 Å that are typical dative U-O bond distances.[41] Removal of the "London-Bridge" 12C4 from **A** enables better coordination by the remaining 12C4 in **B**. The $O_{yl}UO_{yl}$ moiety in **B** is bent from linearity to 154.1°, though the U-O_{yl} distances of ~1.76 Å are typical of uranyl. The uranyl ν_1 of ca. 971 cm^{-1} is slightly red-shifted from that of **A**, 981 cm^{-1}, suggesting more charge donation from two 12C4 in **B** versus three in **A**.[74]

Spontaneous water addition to **B** occurs by reactions (3) and (4). From energies and structures in Table S5 it is apparent that in trans-$[(12C4)(UO_2)(O_2)(UO_2)(12C4)(H_2O)_2]^{2+}$ isomer, *trans*-**B**.2H_2O, the two exposed uranyl sites are hydrated. The *cis*-**B**.2H_2O structure has more steric repulsion between 12C4 ligands and is ca. 6 kcal/mol higher energy. Like the *sandwich* structure of $[UO_2(12C4)_2]^{2+}$,[19] *trans*-**B**.2H_2O has two highly coordinated uranium centers. Dissociative chemisorption of two H_2O to **B** is computed to yield a higher energy hydroxide, as detailed in Table S5.

Hydration of the two uranyl centers in **B**.2H_2O induces U-O_{yl} bond elongations of only ca. 0.002 Å. Notably, addition of two waters to **B** results in a blue-shift of the uranyl ν_1 mode by ~ 3 cm^{-1} to 974 cm^{-1} in **B**.2H_2O. This small shift suggests diminished net charge donation upon hydration, which can be attributed to a change from tetradentate to tridentate 12C4 coordination. In **B**.2H_2O both U centers have three U-O_L dative bonds with bond distances less than 3 Å. In both **B** and **B**.2H_2O the quasi-equatorial uranyl coordination is limited to six due to steric constraints.

The energies for reactions 3 and 4 are nearly the same, to within 1 kcal/mol (Table 1). This contrasts to addition of water to UO_2^+, for which the second hydration is ca. 4 kcal/mol less exothermic than the first.[41] Sequential water addition to monomeric uranyl becomes decreasingly favorable as donor atoms reduce the charge on uranium. In contrast, sequential addition of two waters to **B** occurs at separated U(VI) such that the binding of the second is minimally affected by the first, which results in comparable first and second hydration energies.

Binding of 12C4 to **A** and **B** was investigated using chemical bonding analyses. Results in Table S9 for energy decomposition analysis (EDA) based on Kohn-Sham canonical molecular orbitals (CMOs) show significant energy contributions to U-12C4 bonding from both electrostatic and orbital (covalent) interactions. From EDA and EDA-NOCV, the covalent character in **A** can be understood in terms of 12 dominant density deformation channels, $\Delta\rho_1(r)$ to $\Delta\rho_{12}(r)$, which arise from ligand-to-metal donation (Table S9, Figure S6); these interactions provide total stabilization of −213.82 kcal/mol. The covalent interaction between $[(UO_2)(O_2)(UO_2)]^{2+}$ and two 12C4 ligands in **B** is deconvoluted into dominant channels $\Delta\rho_k(r)$ (k = 1, 2, …, 10), with respective orbital energetic stabilizations (kcal/mol) of −14.18, −13.69, −14.09, −14.04, −8.65, −7.94, −9.42, −9.42, −5.37 and −5.53. The total interaction energy yields 69 kcal/mol for cleavage of a 12C4 ligand from **A**, which is similar to the energy for reaction (1) (57 kcal/mol). Atomic charge analysis gives an average charge of -0.49 on O_L in **B**, versus -0.45 on O_L in **A**.

Structure of $[(UO_2)_2(12C4)_2]^{2+}$ (C): A "Cation-Cation" Interaction

CID of **B** resulted in loss of O_2 to yield **C**, which we tentatively designate as $[(12C4)(UO_2)(UO_2)(12C4)]^{2+}$. Although it is tempting to speculate that the eliminated O_2 is the bridging dioxo moiety, there is no mechanistic evidence for this. The following discussion reveals that representation of **C** as a uranyl dimer is a gross oversimplification. The computed energy for conversion of **B** to **C** via CID reaction (2) is 68 kcal/mol. Addition of one and two waters to **C**, reactions (5) and (6), is exothermic by 14 and 18 kcal/mol, respectively

The valence electronic configuration of **C** based on the singly occupied molecular orbital (SOMO) is $U(5f^1)$-$U(5f^1)$, indicating that both are U(V) as inferred from chemical composition. The structure of **C** corresponds to elimination of O_2 from **B** to yield a $(UO_2)_2^{2+}$ core. The short U-O_t bond lengths in **C** of 1.804 Å are similar to other complexes of pentavalent U. In **C** one O_L atom yields a nearly linear O_L-U-O_t (angle = 169°) but the U-O_L distance of 2.57 Å is characteristic of a dative bond and is only slightly shorter than other U-O_L (2.63-2.72 Å). The U-O_b bond lengths in **C**, 2.11 Å, are shorter than in **A** and **B** (2.28-2.37 Å), and the O_b-O_b distance in **C**, 2.50 Å, is much longer than in **A** and **B** (1.46 Å). The distances in **C** indicate absence of an O_b-O_b bond, and a U(V)-U(V) interaction that is an unusual CCI in which the uranyl moieties have been essentially destroyed (Schemes 1d and 2). The U-U distance in **C**, 3.39 Å, is shorter than in **A** (4.24 Å) and **B** (4.36 Å). A key difference between the $[(UO_2)(O_2)(UO_2)]^{2+}$ moieties in **A** and **B**, versus $[(UO_2)_2]^{2+}$ in **C** , is the deviation from quasi-linear $O_{yl}UO_{yl}$ in **A** (174°) and **B** (154°), to extremely bent O_tUO_b in **C** (102°). The vibrational mode that corresponds to the uranyl ν_1 symmetric stretch mode in **C** is at 881 cm^{-1} which is ~100 cm^{-1} lower energy than ν_1 in **A** and **B**, and is similar to that reported for uranyl(V).[34]

To evaluate magnetic properties of **C**, two configurations of the $[(UO_2)_2]^{2+}$ core were considered: high-spin (HS-**C**) triplet (S = 1) with ferromagnetic f^{α}–f^{α} coupling, and unrestricted broken-symmetry (BS-**C**) singlet (S = 0) with antiferromagnetic f^{α}–f^{β} coupling. The B3LYP and PBE optimized structures of BS-**C** are identical to those of HS-**C** (Table S6). HS-**C** is computed to be only 0.01 kcal/mol (ca. 4 cm^{-1}) higher energy than BS-**C**, indicating minimal magnetic coupling. The exchange coupling constant *J* between the two U(V) is estimated as 6.9 cm^{-1} from the following:[75] $J = (E_{BS} - E_{HS})/(\langle S^2\rangle_{HS} - \langle S^2\rangle_{BS})$, where $E_{BS} - E_{HS}$ is the energy difference between HS and BS, and $\langle S^2\rangle_{HS}$ and $\langle S^2\rangle_{BS}$ are the mean values of the $\hat{S}^2$ spin operators. The frontier MO diagrams for HS-**C** and BS-**C** are the same, except for the highest occupied MOs. For HS-**C** (Figure 6), the two α SOMO and SOMO-1 are localized on the two U(V) spin centers, bearing ferromagnetic $5f^1$–$5f^1$ character. Similarly, one pair of antiferromagnetic spin HOMO-α and HOMO-β molecular levels are distinguished for the BS state. The uranium 5f orbital percentages of these MOs are: 93.1% for SOMO and 95.5% for SOMO−1 in HS-**C**, and 95.2% for HOMO-α and 95.1% for HOMO-β in BS-**C**. Consequently, these MOs exhibit negligible magnetic coupling between U(V) centers.

In GS **C**.H_2O the O_w binds side-on to the U(V) center as shown in Table S7; this structure is 5 kcal/mol lower energy than with O_w binding top-on. The hydroxide isomers are higher energy, by 4.6 and 11.5 kcal/mol for **C**.H_2O and **C**.$2H_2O$, respectively. Products of reactions (5) and (6) are thus

assigned as hydrates rather than hydroxides. Addition of H_2O to **C** elongates the U-O_{yl} bond length, with concomitant red-shifting of the uranyl ν_1 vibrational mode to ca. 852 cm^{-1}, indicating U-O_{yl} bond weakening upon hydration.

The energies for reactions (5) and (6) in Table 1 suggest that hydration of **C** is more exothermic for the second versus the first water molecule, which is the opposite of the trend for bare uranyl(V).[41] Although the energy difference between the first and second hydrations of **C** is modest (1.7 kcal/mol at PBE; 3.7 kcal/mol at B3LYP), it is considered outside of computational error. A more substantial energy difference is apparent for hydration of **B** versus **C**, with the former ~10 kcal/mol more exothermic, a trend reported for bare uranyl(VI) and uranyl(V). However, both the hydration energies, -68.4 kcal/mol for UO_2^{2+} and -36.1 kcal/mol for UO_2^{+}, and the difference between them (~32 kcal/mol) are greater for bare uranyl compared with **B** and **C**.[76] As reported for other uranyl complexes,[41] donor ligands such as 12C4 in **B** and **C** decrease the effective charge on the uranium center, which decreases electrostatic interaction with coordinating waters.

Elaborating the "Cation-Cation" Interaction in $[(UO_2)_2(12C4)_2]^{2+}$ (C)

A particularly remarkable result is CID elimination of O_2 from bridging-peroxide dimer **B** to yield **C**. This contrasts with previous results for CID of uranyl(VI) peroxide complex $[(DMA)(UO_2)(O_2)(UO_2)(DMA)]^{2+}$ (DMA is defined above) to yield U(V) complex $[(DMA)(UO_2)]^{+}$ and U(VI) superoxide $[(DMA)(UO_2)(O_2)]^{+}$.[71] Our calculations indicate that conversion of **B** gives **C** occurs with reduction of both U(VI) to U(V). Reaction (2) can be formulated as (2') in which the bridging O_2 is eliminated while retaining the +2 charge and dimeric structure, by creating a direct unmediated CCI interaction between two U(V) moieties. In reaction (2)/(2'), the U(VI) are reduced to U(V) while O_2^{2-} is oxidized to O_2. It should be noted that there is no mechanistic evidence that the eliminated O_2 is the bridging peroxide; only the net reaction is definitively established.

$[(12C4)(UO_2^{2+})(O_2^{2-})(UO_2^{2+})(12C4)]$ (**B**) → $[(12C4)(UO_2^{+})(UO_2^{+})(12C4)] + O_2$ (**C**) (2')

In Scheme 1 are simplified structures for CCIs between two U(V) moieties. Structures (a) and (b) are typical condensed phase CCIs.[25, 77] Structure (c) is a cis-dioxido uranyl configuration as alleged to form in a coordination polymer,[78] a claim that has been disputed.[79] In structure (d) the uranyl moieties have been disrupted to such an extent—actually destroyed—that a better description is two terminal U=O_t linked by two bridging O_b. Although O-atom bridging of intact uranyls is well known,[80-81] such uranyl destruction is not. The structural parameters for **C** indicate a core as in (d), though with both U also coordinated by a 12C4. The U=O_t distances in **C**, 1.80 Å at the B3LYP level (1.827 Å at PBE), are consistent with typical U=O_{yl} distances, and the U-O_b distances, 2.11 Å, are similar to typical U-O single bond distances, such as terminal U-OH[41] and bridging U-O_b-U.[71]

The basis for the semi-empirical bond-valence approach to estimating oxidation states was described 90 years ago by Pauling,[82] and subsequently elaborated by Brown.[83-85] Like other such sound and persistent models, bond-valence is necessarily somewhat qualitative but has proved sufficiently valid that it remains relevant. Although developed in the context of extended solids, the method is also

applicable to molecules.[86] The bond-valence approach is employed here to evaluate U-O bonds in **C** using the B3LYP bond distances (Table S6), a U-O bond valence parameter of 2.10 Å,[87] and universal constant B = 0.37 Å.[88] This assessment provides the following bond valences in **C**: 2.23 for U-O_t; 0.97 for both U-O_b; and 0.28, 0.24, 0.22 and 0.19 for the four U-O_L. Notably, the sum of these bond valences provides an oxidation states of 5.1 for both U in **C**. The remarkably good agreement of this assessment with the assignment as U(V) may be somewhat fortuitous, but is nonetheless notable.

To assess the role of 12C4 in inducing the extreme CCI in **C** we consider reactions 7 and 8 for formation of a U(V) CCI with and without terminal 12C4. The computed energy (kcal/mol) for reaction (7) is -18.1 at PBE level and -21.1 at B3LYP; that for (8) is 35.6 at PBE and 46.4 at B3LYP.

$2[(12C4)(UO_2^+)] \rightarrow [(12C4)(UO_2^+)(UO_2^+)(12C4)]$ (**C**) (7)

$2(UO_2^+) \rightarrow [(UO_2^+)(UO_2^+)]$ (8)

Referring to the structures in Scheme 1, in distinct contrast to (d) found in **C**, the most stable bare CCI product of reaction (8) is side-on structure (b). Peterson and co-workers reported coupled cluster computations for gas-phase actinyl CCIs, including an energy of 40.3 kcal/mol for reaction (8); the T-shaped structure (a) was also computed there and found to be 9.9 kcal/mol less stable.[89] Both the previous and the present results indicate that the bare U(V)-U(V) CCI is inherently unstable towards Coulomb dissociation. Our results for reaction (7) reveal that coordinating 12C4 ligands induce the extreme CCI structure (d) in **C**, which, unlike bare U(V)-U(V), is thermodynamically stable. The structure of $[(UO_2)(12C4)]^+$ in Scheme 2 reveals that 4-coordinate 12C4 ligands distort the $O_{yl}UO_{yl}$ moiety from linear to 144°. Fusion of two $[(UO_2)(12C4)]^+$ yield **C** results in a more radical deviation from linear, to 102°, with conversion of two of the U=O_{yl} to U-O_b, and the other two to U=O_t. The structure and stability of **C** is attributed to strong U-O_L bonding, which are minimally disrupted in reaction (7). In **C**, both uranium centers are 7-coordinate with one U=O_t double bond, two U-O_b single bonds, and four U-O_L dative bonds. It is evidently favorable to maintain such high U coordination, at the expense of destruction of the $O_{yl}UO_{yl}$ moiety.

Structure (b) in Scheme 1, which appears for bare $[(UO_2^+)(UO_2^+)]$, has two intact $O_{yl}UO_{yl}$ moieties, while in **C** they are converted to structure (d) with bridge-linked $[O=U(-O_b)_2]^+$. Considering the cleaved and created bonds, transition of (b) to (d) is comparable to isomerization of hydrated actinyl, $(H_2O)(AnO_2^+)$, to hydroxide $[O=An(OH)_2]^+$.[76, 90] Energies for these hydrolytic isomerizations, ΔH(hydrol), have been reported as follows (in kcal/mol):[76] 0 for An = Pa; 12 for An = U; 21 for An = Np; 28 for An = Pu; 36 for An = Am. Hydrolytic conversion of an An=O_{yl} to two An-OH is analogous to transformation of CCI structure (b) to (d) (Scheme 1). Thus, PaO_2^+ is predicted to be most prone to disruption of (b) to yield **C**, with AmO_2^+ less prone by ~36 kcal/mol relative to PaO_2^+; **C** and related structures should be most stable for PaO_2^+ and least so for AmO_2^+.

Conclusions

Multidentate O-donor ligand 12C4 yields new bonding motifs and structures in gas-phase uranyl

dimers. $[(UO_2)_2(O_2)(12C4)_3]^{2+}$ (**A**) consists of two U(VI) coordinated by a terminal 12C4 and linked by a peroxide. The third "extra" 12C4 ligand in **A** forms an O-anchored "London Bridge" between the U centers; elimination of this bridging 12C4 requires 56 kcal/mol and yields conventional U(VI) peroxide dimer $[(UO_2)_2(O_2)(12C4)_2]^{2+}$ (**B**). Elimination of the bridging O_2 from **B** yields $[(UO_2)_2(12C4)_2]^{2+}$ (**C**), concomitant with reduction of U(VI) to U(V). In **C** the uranyl moieties have been destroyed in an extreme U(V) CCI, with two O_{yl} converted to bridging, U-O_b-U. Because transformation of **B** to **C** is essentially similar to isomerization of the molecular hydrate $(H_2O)UO_2^+$ to hydroxide $OU(OH)_2^+$, we predict that an An(V) CCI like in **C** should also be accessible for Pa(V), but not for Am(V). Notably, it is not the absolute strength of the disrupted actinyl bonds in an O_{yl}=An=O_{yl} moiety that governs the ease of transformation to An-O_b single bonds, but rather the difference in the energies of the An=O_{yl} versus An-O_b bonds.

As complex **A** was produced in high abundance by ESI, it is tempting to speculate that it may exist in solution. A major caveat to any such interpretation is that the ESI path from solution to gas is sufficiently perturbing that coalescence of two monomers into a dimer with an inter-uranyl 12C4 bridge could occur as a result of desolvation. Spectroscopic evidence would be needed to directly identify species **A** in solution. Given that **A** may not be an important aqueous solution species due to competition for coordination of the uranium centers by solvent molecules like water, rather than by 12C4, a general approach for promoting formation of **A** in solution would be to employ a weakly coordinating solvent.

In addition to demonstrating a novel U(V) CCI, the coordination chemistry in **C** may ultimately guide bulk synthesis of such bonding motifs. In this regard it should be noted that the binding energy between two $[(12C4)(UO_2^+)]$, only ~21 kcal/mol, is likely insufficient to induce such disruption of uranyl moieties in condensed phase. Given that the multidentate 12C4 oxygen donor ligands substantially stabilize **C**—relative to a CCI between bare UO_2^+—more strongly binding ligands might further facilitate such structurally extreme CCIs. Structure **C** for actinyls in general is feasible if the energy to destroy the O_{yl}=An=O_{yl} moiety is offset by the energy for formation of the two resultant U-O_b bonds, a compensation that would be enhanced by destabilizing the parent actinyl moiety and/or stabilizing the bridged oxo product. Robust and sterically demanding multidentate coordination by 12C4 destabilizes the actinyl motif, as revealed by a substantial deviation from linearity in mononuclear $(12C4)UO_2^+$. Other more strongly chelating ligands might destabilize the actinyl structure even more, thereby supporting formation of an oxo-bridging CCI as in **C**. Another strategy for disrupting an actinyl moiety is by anion coordination, such as for example by a carboxylate $RCOO^-$ in mononuclear $[(L)(RCOO)An^{VI}O_2]^+$, where L denotes a supporting neutral ligand(s). If the actinyl is sufficiently disturbed, coalescence of two such monocations could yield oxo-bridged An(VI) CCI $[(L)(RCOO)(An^{VI}O_2)(An^{VI}O_2)(RCOO)(L)]^{2+}$.

Supporting Information

ESI mass spectrum of UO_2Cl_2:12C4. High m/z portion of CID mass spectrum for **A**. Mass spectra of selected species with and without acetonitrile gas added to the ion trap. Plots of representative $U-O_L$ bonding in **A**, **B** and **C** from EDA-NOCV analyses. Computed energies of GS species cited in Tables 1 and 2. Relative energies, selected bond lengths, and bond angles for isomers of **A**, **B** and **C** and hydrates, and for high-spin and low-spin **C**. EDA and EDA-NOCV analyses. Bond orders, charges, and geometrical coordinates for GS species.

Acknowledgements

The experimental work was fully supported by the Center for Actinide Science and Technology (CAST), an Energy Frontier Research Center (EFRC) funded by the U.S. Department of Energy (DOE), Office of Science, Basic Energy Sciences (BES), under Award Number DE-SC0016568 [J.J. and J.K.G.]. The computational work was financially supported by the NASF (No. U1530401), and by the Foundation of President of China Academy of Engineering Physics (No. YZJJSQ2017072), and by the National Natural Science Foundation of China (NSFC Nos. 91426302, 21433005 and 21701006) [J.L. and S.X.H]. The calculations were performed at the Tsinghua National Laboratory for Information Science and Technology, and at the Tianhe2-JK, China.

References

1. Steele, H.; Taylor, R. J., A Theoretical Study of the Inner-Sphere Disproportionation Reaction Mechanism of the Pentavalent Actinyl Ions. *Inorganic Chemistry* **2007,** *46*, 6311−6318.
2. Arnold, P. L.; Love, J. B.; Patel, D., Pentavalent uranyl complexes. *Coordination Chemistry Reviews* **2009,** *253*, 1973−1978.
3. Faizova, R.; White, S.; Scopelliti, R.; Mazzanti, M., The effect of iron binding on uranyl(v) stability. *Chemical Science* **2018,** *9*, 7520−7527.
4. Katz, J. J.; Seaborg, G. T.; Morss, L. R., The Chemistry of the Actinide Elements. 2 ed.; Springer Netherlands: 1986; Vol. 1, pp XII, 990.
5. Li, Y.; Su, J.; Mitchell, E.; Zhang, G.; Li, J., Photocatalysis with visible-light-active uranyl complexes. *Science China Chemistry* **2013,** *56*, 1671−1681.
6. Renshaw, J. C.; Butchins, L. J. C.; Livens, F. R.; May, I.; Charnock, J. M.; Lloyd, J. R., Bioreduction of Uranium: Environmental Implications of a Pentavalent Intermediate. *Environmental Science and Technology* **2005,** *39*, 5657−5660.
7. Kolarik, Z., Complexation and separation of lanthanides(III) and actinides(III) by heterocyclic N-donors in solutions. *Chemical reviews* **2008,** *108*, 4208−4252.
8. Dam, H. H.; Reinhoudt, D. N.; Verboom, W., Multicoordinate ligands for actinide/lanthanide separations. *Chemical Society reviews* **2007,** *36*, 367−377.
9. Kubatko, K. A. H.; Helean, K. B.; Navrotsky, A.; Burns, P. C., Stability of peroxide-containing uranyl minerals. *Science* **2003,** *302*, 1191−1193.
10. Arnold, P. L.; Pecharman, A. F.; Hollis, E.; Yahia, A.; Maron, L.; Parsons, S.; Love, J. B., Uranyl oxo activation and functionalization by metal cation coordination. *Nat Chem* **2010,** *2*, 1056-1061.
11. Lan, J.-H.; Shi, W.-Q.; Yuan, L.-Y.; Li, J.; Zhao, Y.-L.; Chai, Z.-F., Recent advances in computational modeling and simulations on the An(III)/Ln(III) separation process. *Coordination Chemistry Reviews* **2012,** *256*, 1406−1417.

12. Panak, P. J.; Geist, A., Complexation and extraction of trivalent actinides and lanthanides by triazinylpyridine N-donor ligands. *Chem Rev* **2013,** *113*, 1199−1236.
13. Veliscek-Carolan, J., Separation of actinides from spent nuclear fuel: A review. *Journal of hazardous materials* **2016,** *318*, 266−281.
14. Swidan, A. a.; Macdonald, C. L. B., Polyether complexes of groups 13 and 14. *Chemical Society reviews* **2016,** *45*, 3883−3915.
15. Alexander, V., Design and synthesis of macrocyclic ligands and their complexes of lanthanides and actinides. *Chemical reviews* **1995,** *95*, 273−342.
16. Gorden, A. E. V.; Xu, J. D.; Raymond, K. N.; Durbin, P., Rational design of sequestering agents for plutonium and other actinides. *Chemical reviews* **2003,** *103*, 4207−4282.
17. Hu, S.-X.; Li, W. L.; Dong, L.; Gibson, J. K.; Li, J., Crown ether complexes of actinyls: a computational assessment of AnO_2(15-crown-5)$^{2+}$ (An = U, Np, Pu, Am, Cm). *Dalton Transactions* **2017,** *46*, 12354−12363.
18. Hu, S.-X.; Liu, J.-J.; Gibson, J. K.; Li, J., Periodic trends in actinyl thio-crown ether complexes. *Inorganic Chemistry* **2018**.
19. Hu, S. X.; Gibson, J. K.; Li, W. L.; Van Stipdonk, M. J.; Martens, J.; Berden, G.; Redlich, B.; Oomens, J.; Li, J., Electronic structure and characterization of a uranyl di-15-crown-5 complex with an unprecedented sandwich structure. *Chemical Communications* **2016,** *52*, 12761−12764.
20. Jian, J.; Hu, S.-X.; Li, W.-L.; van Stipdonk, M. J.; Martens, J.; Berden, G.; Oomens, J.; Li, J.; Gibson, J. K., Uranyl/12-crown-4 Ether Complexes and Derivatives: Structural Characterization and Isomeric Differentiation. *INORGANIC CHEMISTRY* **2018,** *57*, 4125−4134.
21. Stoyer, N. J.; Hoffman, D. C.; Silva, R. J., Cation-cation complexes of PuO_2^+ and NpO_2^+ with Th^{4+} and UO_2^{2+}. *Radiochim Acta* **2000,** *88*, 279.
22. Niklas, J. E.; Farnum, B. H.; Gorden, J. D.; Gorden, A. E. V., Structural Characterization and Redox Activity of a Uranyl Dimer and Transition-Metal Complexes of a Tetradentate BIAN Ligand. *Organometallics* **2017,** *36*, 4626−4634.
23. Fromager, E.; Vallet, V.; Schimmelpfennig, B.; Macak, P.; Privalov, T.; Wahlgren, U., Spin−Orbit Effects in Electron Transfer in Neptunyl(VI)−Neptunyl(V) Complexes in Solution. *Journal of Physical Chemistry A* **2005,** *109*, 4957−4960.
24. Burdet, F.; Pecaut, J.; Mazzanti, M., Isolation of a tetrameric cation-cation complex of pentavalent uranyl. *J. Am. Chem. Soc.* **2006,** *128*, 16512−16513.
25. Nocton, G.; Horeglad, P.; Pecaut, J.; Mazzanti, M., Polynuclear Cation-Cation Complexes of Pentavalent Uranyl: Relating Stability and Magnetic Properties to Structure. *J. Am. Chem. Soc.* **2008,** *130*, 16633−16645.
26. Hamon, N.; Galland, M.; Le Fur, M.; Roux, A.; Duperray, A.; Grichine, A.; Andraud, C.; Le Guennic, B.; Beyler, M.; Maury, O.; Tripier, R., Combining a pyclen framework with conjugated antenna for the design of europium and samarium luminescent bioprobes. *Chemical Communications* **2018,** *54*, 6173−6176.
27. Guillaume, B.; Begun, G. M.; Hahn, R. L., Raman Spectrometric Studies of Cation Cation Complexes of Pentavalent Actinides in Aqueous Perchlorate Solutions. *Inorganic Chemistry* **1982,** *21*, 1159-1166.
28. Vasiliu, M.; Gibson, J. K.; Peterson, K. A.; Dixon, D. A., Gas Phase Hydrolysis and Oxo-Exchange of Actinide Dioxide Cations: Elucidating Intrinsic Chemistry from Protactinium to Einsteinium. *Chem-Eur J* **2019,** *25*, 4245-4254.
29. Charushnikova, I. A.; Krot, N. N.; Starikova, Z. A., Cation–cation interaction in crystal structures of Np(V) and Pu(V) benzoate complexes with 2,2′-bipyridine, $[NpO_2(C10H8N2)(OOCC_6H_5)]_2$ and $[PuO_2(C_{10}H_8N_2)(OOCC_6H_5)]_2$. *Radiochim Acta* **2007,** *95*, 495-499.
30. Serezhkin, V. N.; Sidorenko, G. V.; Pushkin, D. V.; Serezhkina, L. B., Cation-cation interactions between uranyl(VI) ions. *Radiochemistry* **2014,** *56*, 115−133.
31. Barbanel, Y. A.; Dushin, R. B.; Kolin, V. V.; Kotlin, V. P.; Mashirov, L. G.; Nekhoroshkov, S. N., First Observation of the Cation-Cation Interaction of Actinides in Melts: NpO_2^+-UO_2^{2+} System. *Radiochemistry* **2003,** *45*, 276−278.

32. Burn, A. G.; Martin, L. R.; Nash, K. L., Pentavalent Neptunyl ([O≡Np≡O]$^{+}$) Cation–Cation Interactions in Aqueous/Polar Organic Mixed-Solvent Media. *Journal of Solution Chemistry* **2017,** *46*, 1299−1314.
33. Mougel, V.; Biswas, B.; Pécaut, J.; Mazzanti, M., New insights into the acid mediated disproportionation of pentavalent uranyl. *Chemical Communications* **2010,** *46*, 8648−8650.
34. Privalov, T.; Macak, P.; Schimmelpfennig, B.; Fromager, E.; Grenthe, I.; Wahlgren, U., Electron Transfer in Uranyl(VI)−Uranyl(V) Complexes in Solution. *J. Am. Chem. Soc.* **2004,** *126*, 9801−9808.
35. Armstrong, C. R.; Nyman, M.; Shvareva, T.; Sigmon, G. E.; Burns, P. C.; Navrotsky, A., Uranyl peroxide enhanced nuclear fuel corrosion in seawater. *Proceedings of the National Academy of Sciences* **2012,** *109*, 1874−1877.
36. Miró, P.; Vlaisavljevich, B.; Gil, A.; Burns, P. C.; Nyman, M.; Bo, C., Self-Assembly of Uranyl-Peroxide Nanocapsules in Basic Peroxidic Environments. *Chemistry-A European Journal* **2016,** *22*, 8571−8578.
37. Zhang, Y.; Bhadbhade, M.; Price, J. R.; Karatchevtseva, I.; Kong, L.; Scales, N.; Lumpkin, G. R.; Li, F., Uranyl peroxide clusters stabilized by dicarboxylate ligands: A pentagonal ring and a dimer with extensive uranyl–cation interactions. *Polyhedron* **2015,** *92*, 99−104.
38. Odoh, S. O.; Shamblin, J.; Colla, C. A.; Hickam, S.; Lobeck, H. L.; Lopez, R. A. K.; Olds, T.; Szymanowski, J. E. S.; Sigmon, G. E.; Neuefeind, J.; Casey, W. H.; Lang, M.; Gagliardi, L.; Burns, P. C., Structure and Reactivity of X-ray Amorphous Uranyl Peroxide, U_2O_7. *Inorganic Chemistry* **2016,** *55*, 3541−3546.
39. Zanonato, P. L.; Di Bernardo, P.; Vallet, V.; Szabó, Z.; Grenthe, I., Alkali-metal ion coordination in uranyl(vi) poly-peroxide complexes in solution. Part 1: the Li^+, Na^+ and K^+ – peroxide–hydroxide systems. *Dalton Transactions* **2015,** *44*, 1549−1556.
40. Sullivan, J. C.; Zielen, A. J.; Hindman, J. C., Specific Interaction between Np(V) and U(Vi) in Aqueous Perchloric Acid Media. *J. Am. Chem. Soc.* **1961,** *83*, 3373-&.
41. Rios, D.; Michelini, M. C.; Lucena, A. F.; Marcalo, J.; Bray, T. H.; Gibson, J. K., Gas-Phase Uranyl, Neptunyl, and Plutonyl: Hydration and Oxidation Studied by Experiment and Theory. *Inorg Chem* **2012,** *51*, 6603-6614.
42. Gong, Y.; Gibson, J. K., Crown Ether Complexes of Uranyl, Neptunyl, and Plutonyl: Hydration Differentiates Inclusion versus Outer Coordination. *Inorganic Chemistry* **2014,** *53*, 5839-5844.
43. Frisch, M. J.; Trucks, G. W.; Schlegel, H. B.; Scuseria, G. E.; Robb, M. A.; Cheeseman, J. R.; Scalmani, G.; Barone, V.; Mennucci, B.; Petersson, G. A.; Nakatsuji, H.; Caricato, M.; Li, X.; Hratchian, H. P.; Izmaylov, A. F.; Bloino, J.; Zheng, G.; Sonnenberg, J. L.; Hada, M.; Ehara, M.; Toyota, K.; Fukuda, R.; Hasegawa, J.; Ishida, M.; Nakajima, T.; Honda, Y.; Kitao, O.; Nakai, H.; Vreven, T.; Montgomery Jr., J. A.; Peralta, J. E.; Ogliaro, F.; Bearpark, M.; Heyd, J. J.; Brothers, E.; Kudin, K. N.; Staroverov, V. N.; Keith, T.; Kobayashi, R.; Normand, J.; Raghavachari, K.; Rendell, A.; Burant, J. C.; Iyengar, S. S.; Tomasi, J.; Cossi, M.; Rega, N.; Millam, J. M.; Klene, M.; Knox, J. E.; Cross, J. B.; Bakken, V.; Adamo, C.; Jaramillo, J.; Gomperts, R.; Stratmann, R. E.; Yazyev, O.; Austin, A. J.; Cammi, R.; Pomelli, C.; Ochterski, J. W.; Martin, R. L.; Morokuma, K.; Zakrzewski, V. G.; Voth, G. A.; Salvador, P.; Dannenberg, J. J.; Dapprich, S.; Daniels, A. D.; Farkas, Ö.; Foresman, J. B.; Ortiz, J. V.; Cioslowski, J.; Fox, D. J., *Gaussian 09, Revision C.01* **Wallingford CT: Gaussian, Inc. 2010**.
44. Baerends, E. J.; Ellis, D. E.; Ros, P., Self-consistent molecular Hartree-Fock-Slater calculations I. The computational procedure. *Chemical Physics* **1973,** *2*, 41−51.
45. Velde, G. T.; Bickelhaupt, F. M.; Baerends, E. J.; Guerra, C. F.; Van Gisbergen, S. J. A.; Snijders, J. G.; Ziegler, T., Chemistry with ADF. *J. Comput. Chem.* **2001,** *22*, 931−967.
46. Perdew, J. P.; Emzerhof, M.; Burke, K., Rationale for mixing exact exchange with density functional approximations. *J. Chem. Phys.* **1996,** *105*, 9982−9985.
47. van Lenthe, E.; Baerends, E. J., Optimized Slater-type basis sets for the elements 1−118. *J. Comput. Chem.* **2003,** *24*, 1142−1156.

48. van Lenthe, E.; Baerends, E. J.; Snijders, J. G., Relativistic regular 2-component hamiltonians. *J. Chem. Phys.* **1993,** *99*, 4597−4610.
49. Hess, B. A., Relativistic electronic−structure calculations employing a 2−component no-pair formalism with external−field projection operators. *Phys. Rev. A* **1986,** *33*, 3742−3748.
50. Becke, A. D., Density-functional thermochemistry. 3. The role of exact exchange. *J. Chem. Phys.* **1993,** *98*, 5648−5652.
51. Lee, C. T.; Yang, W. T.; Parr, R. G., Development of the Colle-Salvetti correlation-energy formula into a functional of the electron-density. *Phys. Rev. B* **1988,** *37*, 785−789.
52. Cao, X.; Dolg, M., Segmented contraction scheme for small-core actinide pseudopotential basis sets. *Journal of Molecular Structure: THEOCHEM* **2004,** *673*, 203−209.
53. Kendall, R. A.; Dunning Jr., T. H.; Harrison, R. J., Electron affinities of the first-row atoms revisited. Systematic basis sets and wave functions. *J. Chem. Phys.* **1992,** *96*, 6796−6806.
54. Neese, F., Software update: the ORCA program system, version 4.0. *WIREs Computational Molecular Science* **2018,** *8*, e1327.
55. Huang, W.; Xu, W.-H.; Su, J.; Schwarz, W. H. E.; Li, J., Oxidation States, Geometries, and Electronic Structures of Plutonium Tetroxide PuO_4 Isomers: Is Octavalent Pu Viable? *Inorganic Chemistry* **2013,** *52*, 14237−14245.
56. Nalewajski, R. F.; Mrozek, J.; Michalak, A., Two-electron valence indices from the Kohn-Sham orbitals. *International Journal of Quantum Chemistry* **1997,** *61*, 589−601.
57. Michalak, A.; Mitoraj, M.; Ziegler, T., Bond orbitals from chemical valence theory. *Journal of Physical Chemistry A* **2008,** *112*, 1933−1939.
58. Ziegler, T.; Rauk, A., On the calculation of bonding energies by Hartree-Fock slater method. 1. Transition−state method. *Theor. Chim. Acta* **1977,** *46*, 1−10.
59. Ziegler, T.; Rauk, A., A theoretical study of the ethylene-metal bond in complexes between Cu^{1+}, Ag^{1+}, Au^{1+}, Pt^{0} or Pt^{2+} and ethylene, based on the Hartree-Fock-Slater transition-statemethod. *Inorganic Chemistry* **1979,** *18*, 1558−1565.
60. Becke, A. D.; Edgecombe, K. E., A simple measure of electron localization in atomic and molecular systems. *J. Chem. Phys.* **1990,** *92*, 5397−5403.
61. Mayer, I., Charge, bond order and valence in the *ab* inition SCF theory. *Chemical Physics Letters* **1983,** *97*, 270−274.
62. Gopinathan, M. S.; Jug, K., Valency. I. A quantum chemical definition and properties. *Theor. Chim. Acta* **1983** *63*, 497−509.
63. Nalewajski, R. F.; Mrozek, J., Modified valence indices from the two-particle density matrix. *International Journal of Quantum Chemistry* **1994,** *51*, 187−200.
64. Mulliken, R. S., Electronic population analysis on LCAO−MO molecular wave functions. 1. *J. Chem. Phys.* **1955,** *23*, 1833−1840.
65. Hirshfeld, F. L., Bonded-atom fragments for describing molecular charge-densities. *Theor. Chim. Acta* **1977,** *44*, 129−138.
66. Bickelhaupt, F. M.; Hommes, N. J. R. V.; Guerra, C. F.; Baerends, E. J., The carbon-lithium electron pair bond in $(CH_3Li)_n$ (n=1, 2, 4). *Organometallics* **1996,** *15*, 2923−2931.
67. Swart, M.; Van Duijnen, P. T.; Snijders, J. G., A charge analysis derived from an atomic multipole expansion. *J. Comput. Chem.* **2001,** *22*, 79−88.
68. Reed, A. E.; Weinstock, R. B.; Weinhold, F., Natural−population analysis. *J. Chem. Phys.* **1985,** *83*, 735−746.
69. Reed, A. E.; Curtiss, L. A.; Weinhold, F., Intermolecular interactions from a natural bond orbital, donor−acceptor viewpoint. *Chemical reviews* **1988,** *88*, 899−926.

70. Glendening, E. D.; Badenhoop, J., K.; Reed, A. E.; Carpenter, J. E.; Bohmann, J. A.; Morales, C. M.; Landis, C. R.; Weinhold, F. *NBO 6.0.*, Theoretical Chemistry Institute, University of Wisconsin, Madison 2013.
71. Dau, P. D.; Dau, P. V.; Rao, L. F.; Kovacs, A.; Gibson, J. K., A Uranyl Peroxide Dimer in the Gas Phase. *Inorganic Chemistry* **2017,** *56*, 4186−4196.
72. Gronert, S., Estimation of effective ion temperatures in a quadrupole ion trap. *J Am Soc Mass Spectr* **1998,** *9*, 845-848.
73. Lucena, A. F.; Carretas, J. M.; Marcalo, J.; Michelini, M. C.; Gong, Y.; Gibson, J. K., Gas-Phase Reactions of Molecular Oxygen with Uranyl(V) Anionic Complexes-Synthesis and Characterization of New Superoxides of Uranyl(VI). *Journal of Physical Chemistry A* **2015,** *119*, 3628−3635.
74. Gibson, J. K.; de Jong, W. A.; van Stipdonk, M. J.; Martens, J.; Berden, G.; Oomens, J., Equatorial coordination of uranyl: Correlating ligand charge donation with the O-yl-U-O-yl asymmetric stretch frequency. *J Organomet Chem* **2018,** *857*, 94-100.
75. Teyar, B.; Belkhiri, L.; Costuas, K.; Boucekkine, A.; Meyer, K., Electronic Structure and Magnetic Properties of Dioxo-Bridged Diuranium Complexes with Diamond-Core Structural Motifs: A Relativistic DFT Study. *Inorganic Chemistry* **2016,** *55*, 2870−2881.
76. Vasiliu, M.; Peterson, K. A.; Gibson, J. K.; Dixon, D. A., Reliable Potential Energy Surfaces for the Reactions of H_2O with ThO_2, PaO_2^+, UO_2^{2+}, and UO_2^+. *Journal of Physical Chemistry A* **2015,** *119*, 11422−11431.
77. Lachmanska, A.; Tecmer, P.; Legeza, O.; Boguslawski, K., Elucidating cation-cation interactions in neptunyl dications using multi-reference *ab initio* theory. *Phys. Chem. Chem. Phys.* **2019,** *21*, 744−759.
78. Vaughn, A. E.; Barnes, C. L.; Duval, P. B., A cis-dioxido uranyl: Fluxional carboxylate activation from a reversible coordination polymer. *Angew Chem Int Edit* **2007,** *46*, 6622-6625.
79. Villiers, C.; Thuery, P.; Ephritikhine, M., The first cis-dioxido uranyl compound under scrutiny. *Angew Chem Int Edit* **2008,** *47*, 5892-5893.
80. Skanthakumar, S.; Antonio, M. R.; Soderholm, L., A comparison of neptunyl(V) and neptunyl(VI) solution coordination: The stability of cation-cation interactions. *Inorganic Chemistry* **2008,** *47*, 4591−4595.
81. Alekseev, E. V.; Krivovichev, S. V.; Depmeier, W.; Siidra, O. I.; Knorr, K.; Suleimanov, E. V.; Chuprunov, E. V., Na2Li8[(UO2)(11)O-12(WO5)(2)]: Three different uranyl-ion coordination geometries and cation-cation interactions. *Angew Chem Int Edit* **2006,** *45*, 7233-7235.
82. Pauling, L., The principles determining the structure of complex ionic crystals. *J Am Chem Soc* **1929,** *51*, 1010-1026.
83. Brown, I. D., Can We Predict Inorganic Crystal-Structures and Their Properties from Chemical Formula. *Acta Crystallogr A* **1975,** *31*, S60-S60.
84. Brown, I. D., Bond Valences - Simple Structural Model for Inorganic-Chemistry. *Chem Soc Rev* **1978,** *7*, 359-376.
85. Altermatt, D.; Brown, I. D., The Automatic Searching for Chemical-Bonds in Inorganic Crystal-Structures. *Acta Crystallogr B* **1985,** *41*, 240-244.
86. Bickmore, B. R.; Rosso, K. M.; Tadanier, C. J.; Bylaska, E. J.; Doud, D., Bond-valence methods for pK(a) prediction. II. Bond-valence, electrostatic, molecular geometry, and solvation effects. *Geochim Cosmochim Ac* **2006,** *70*, 4057-4071.
87. Zachariasen, W. H., Bond Lengths in Oxygen and Halogen Compounds of D-Element and F-Element. *J Less-Common Met* **1978,** *62*, 1-7.
88. Brese, N. E.; Okeeffe, M., Bond-Valence Parameters for Solids. *Acta Crystallogr B* **1991,** *47*, 192-197.
89. Feng, R.; Glendening, E. D.; Peterson, K. A., Actinyl cation-cation interactions in the gas phase: An accurate thermochemical study. *Phys. Chem. Chem. Phys.* **2019,** *21*, 7953-7964.

90. Rios, D.; Micheini, M. D.; Lucena, A. F.; Marcalo, J.; Gibson, J. K., On the Origins of Faster Oxo Exchange for Uranyl(V) versus Plutonyl(V). *J Am Chem Soc* **2012,** *134*, 15488-15496.

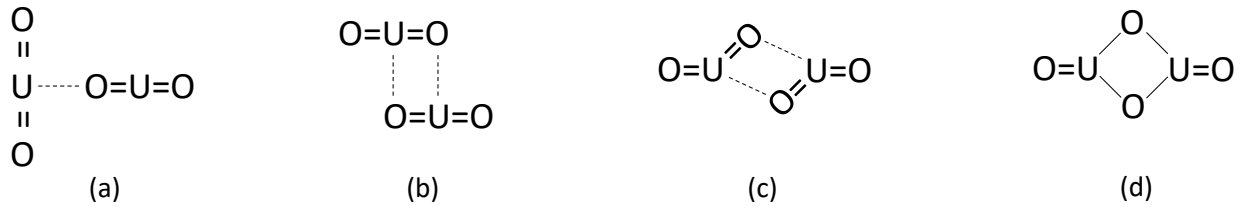

Scheme 1. Possible types of cation-cation interaction between two UO_2^+.

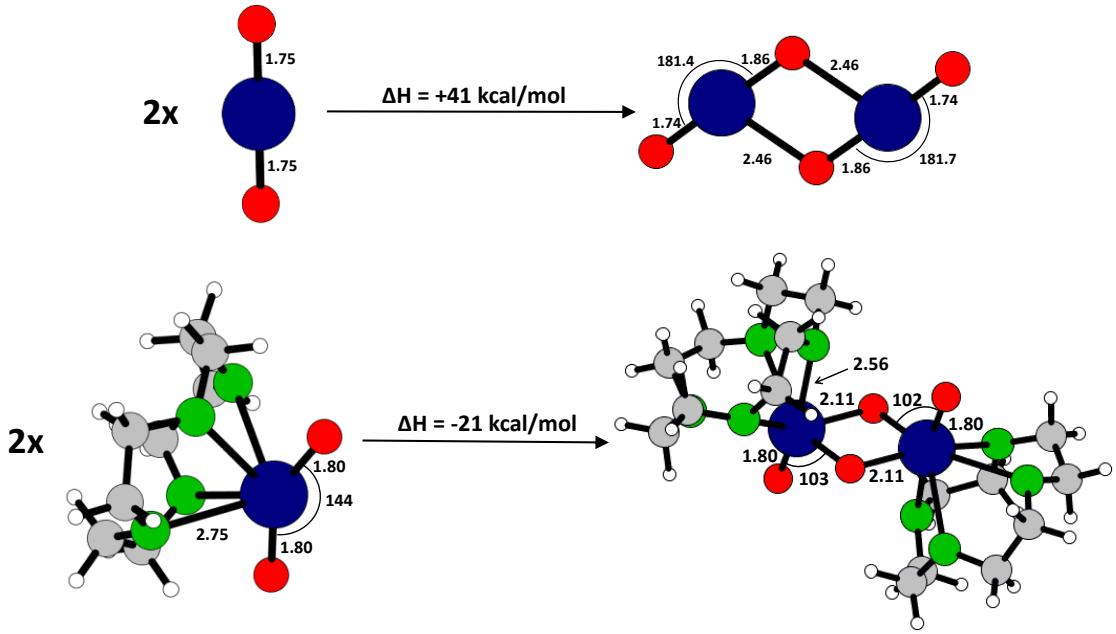

Scheme 2. Computed uranyl(V) CCI structures and energies. Top: Endothermic association of bare UO_2^+. Bottom: Exothermic association of 12C4-coordinated UO_2^+. Bond distances are in Å and angles in degrees.

Table 1. Energy for reactions (1) to (9).[a]

Reaction	ΔH_{PBE}	ΔH_{B3LYP}	$\Delta H_{DLPNO\text{-}CCSD(T)}$
(1)	44.4	56.5	85.8
(2)/(2')	39.6	68.4	97.5
(3)	-21.7	-25.6	-39.9
(4)	-20.7	-25.2	-38.3
(5)	-12.8	-14.4	-27.5
(6)	-14.5	-18.1	-20.4
(7)	-18.1	-21.1	-23.2
(8)	35.6	46.4	41.0

[a]In kcal/mol, using Gaussian B3LYP/ECP60MWB_SEG(U):cc-pVTZ (C, H, O), ADF PBE/TZ2P and Orca DLPNO-CCSD(T)/DKH-def2-TZVP(U):def2-SVP(C,H,O).

Table 2. Energies for addition of 12C4 and H_2O to yield ground-state (GS) adducts.[a]

Species	Config./GS	PBE	B3LYP	DLPNO-CCSD(T)
A[b]	$f^0f^0/^1A$	-223.8	-231.4	-289.5
B[c]	$f^0f^0/^1A$	-179.4	-174.9	-203.7
C[d]	$f^1f^1/^3A$	-206.1	-205.9	-207.5
B.H_2O[c]	$f^0f^0/^1A$	-201.1	-200.5	-243.6
B.$2H_2O$[c]	$f^0f^0/^1A$	-221.7	-225.7	-282.0
C.H_2O[d]	$f^1f^1/^3A$	-219.0	-220.4	-234.9
C.$2H_2O$[d]	$f^1f^1/^3A$	-233.4	-238.5	-255.4

[a]In kcal/mol, with zero-point correction, using ADF PBE/TZ2P, Gaussian B3LYP/ECP60MWB_SEG(U):cc-pVTZ (C, H, O) and Orca DLPNO-CCSD(T)/DKH-def2-TZVP(U):def2-SVP(C,H,O)

[b] Energy for reaction: $3*12C4 + (UO_2)_2O_2^{2+} \rightarrow$ **A**

[c] Energy for reaction: $2*12C4 + (UO_2)_2O_2^{2+} + n\ H_2O \rightarrow$ **B** (n=0); **B**.H_2O (n=1); **B**.$2H_2O$ (n=2)

[d] Energy for reaction: $2*12C4 + [U_2O_4]^{2+} + n\ H_2O \rightarrow$ **C** (n=0); **C**.H_2O (n=1); **C**.$2H_2O$ (n=2)

Table 3. Average bond lengths (Å) and angles (degree) and O_{yl}-U-O_{yl} vibrational stretching frequencies (cm^{-1}, intensity in parentheses) for GS species.[a]

Species[b]	$[(UO_2)_2O_2]^{2+}$	**A**	**B**	**C**	**B**.H_2O	**B**.$2H_2O$	**C**.H_2O	**C**.$2H_2O$
Symmetry	$D_{\infty h}$	C_1	C_1	C_2	C_1	C_2	C_1	C_1
U1-O_{yl}(O_t)	1.722	1.758	1.756	1.804	1.757	1.758	1.815	1.885
U2-O_{yl}(O_t)	1.722	1.759	1.756	1.804	1.756	1.758	1.812	1.885
U1-O_b	2.301	2.328	2.323	2.110	2.349	2.327	2.131	2.319
U2-O_b	2.301	2.334	2.323	2.110	2.306	2.327	2.102	2.317
O_b-O_b	1.460	1.455	1.460	2.508	1.456	1.457	2.504	2.532
U1-U2	4.364	4.242	4.355	3.394	4.262	4.281	3.412	3.468
U1-O_{L1}		2.538	2.775	2.645	2.834	2.860	2.690	2.772
U2-O_{L2}		2.542	2.775	2.645	2.798	2.860	2.662	2.775
U1-O_{L3}		2.542						
U2-O_{L3}		2.503						
U1-O_w					2.500	2.502	2.599	2.557
U2-O_w						2.502		2.561
∠$O_{yl}UO_{yl}$	171.9	173.8	154.1		157.7	161.0		
∠$O_{yl}UO_b$ (∠O_tUO_b)	93.8	92.1	89.1	102.5	88.4	88.8	114.1	143.2
∠$O_{yl}UO_w$					83.0	83.1	76.0	79.4
∠$U_1U_2O_bO_b$	0.0	48.8	26.8	0.0	40.2	39.0	2.7	0.8
v_3	1056.1(0)	970.5(43)	961.8(13)	882.5(0)	961.3(66)	962.5(17)	846.8(87)	851.0(30)
v_1	1062.6(490)	980.9(278)	970.8(422)	881.2(202)	975.1(384)	974.4(47)	852.0(321)	851.4(300)

[a] Using Gaussian B3LYP/ECP60MWB_SEG(U):cc-pVTZ (C, H, O); details are listed in Tables S1, S4, S5 and S6.

[b] L denotes 12C4. O_t denotes terminal U=O_t

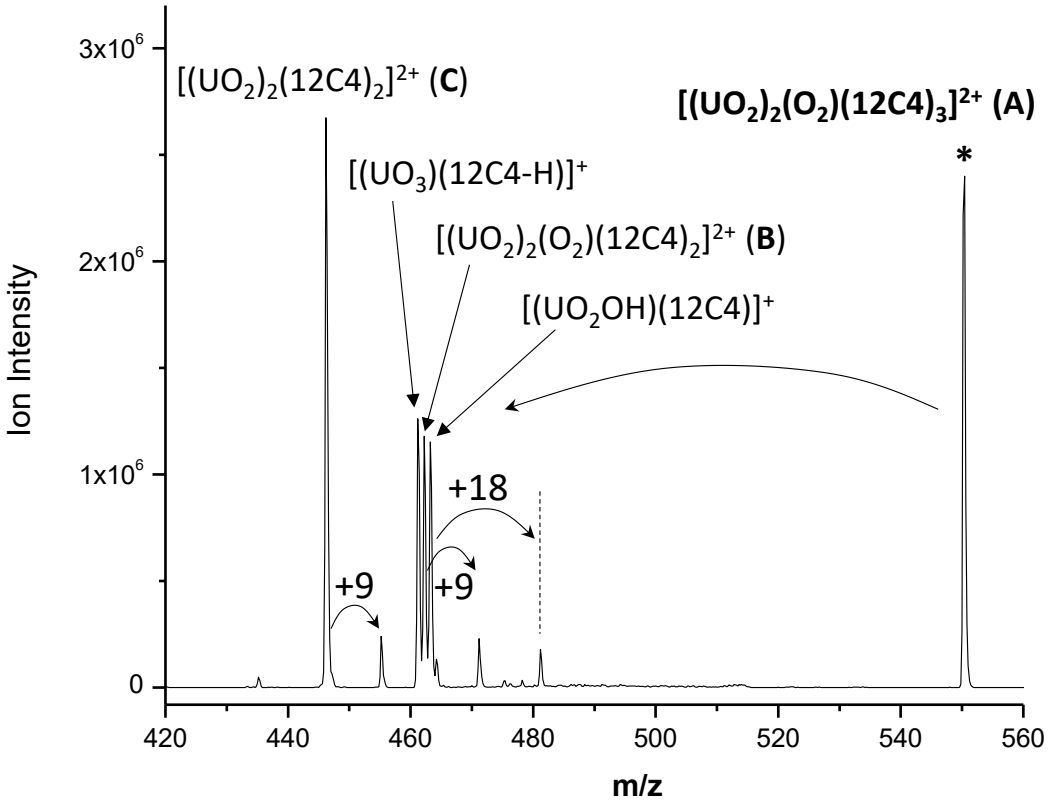

Figure 1. CID mass spectrum of **A** (m/z=550 (0.45V CID; higher m/z products are in Fig. S2). Water addition to CID products yields peaks at +9 m/z for $[(UO_2)_2(12C4)_2]^{2+}$ and $[(UO_2)_2(O_2)(12C4)_2]^{2+}$, and at +18 m/z for $[(UO_2(OH)(12C4)]^{+}$. Formulations do not imply structures.

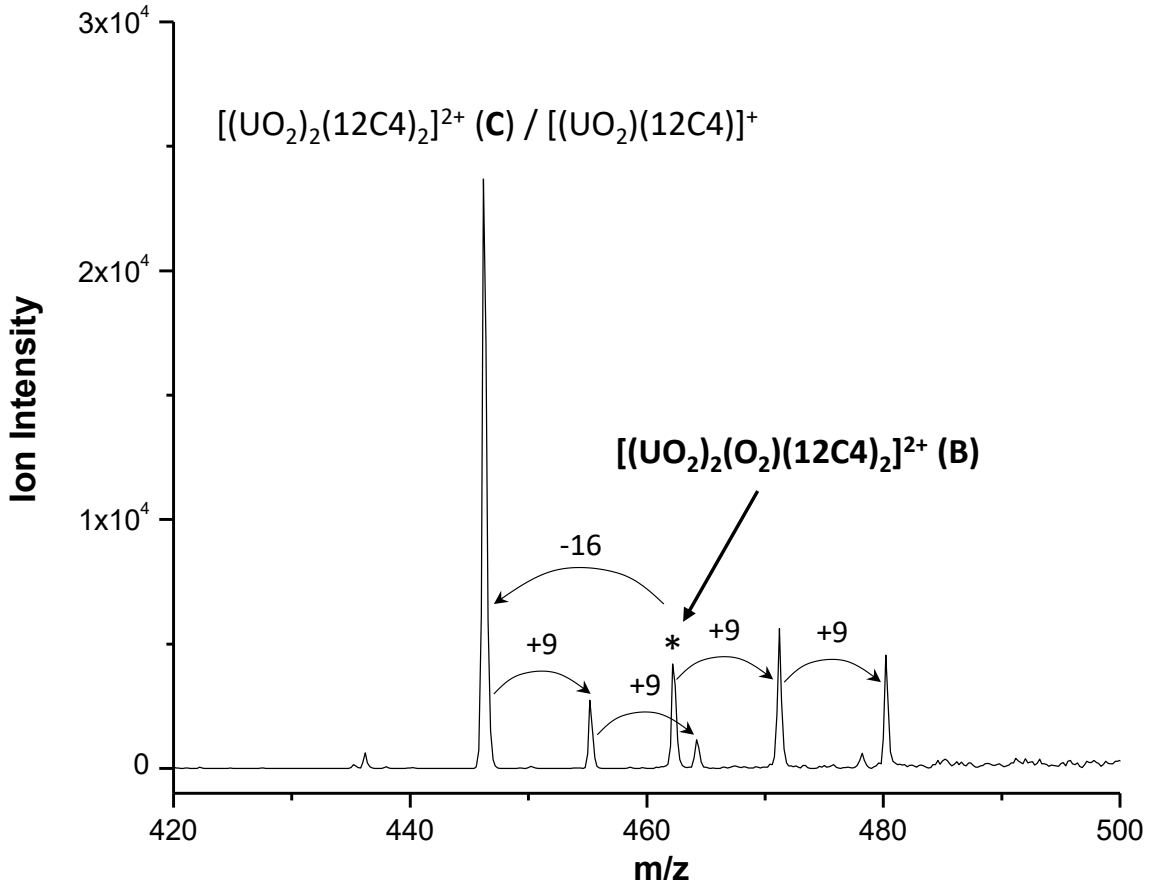

Figure 2. Secondary CID mass spectrum of **B** (m/z= 462; 0.35 V CID) produced by primary CID of **A** (Fig. 2). Dominant CID product $[(UO_2)_2(12C4)_2]^{2+}$ (same m/z as $[(UO_2)(12C4)]^{+}$) results from loss of O_2. Both **B** and its CID product **C** sequentially add two H_2O (+9 m/z for each).

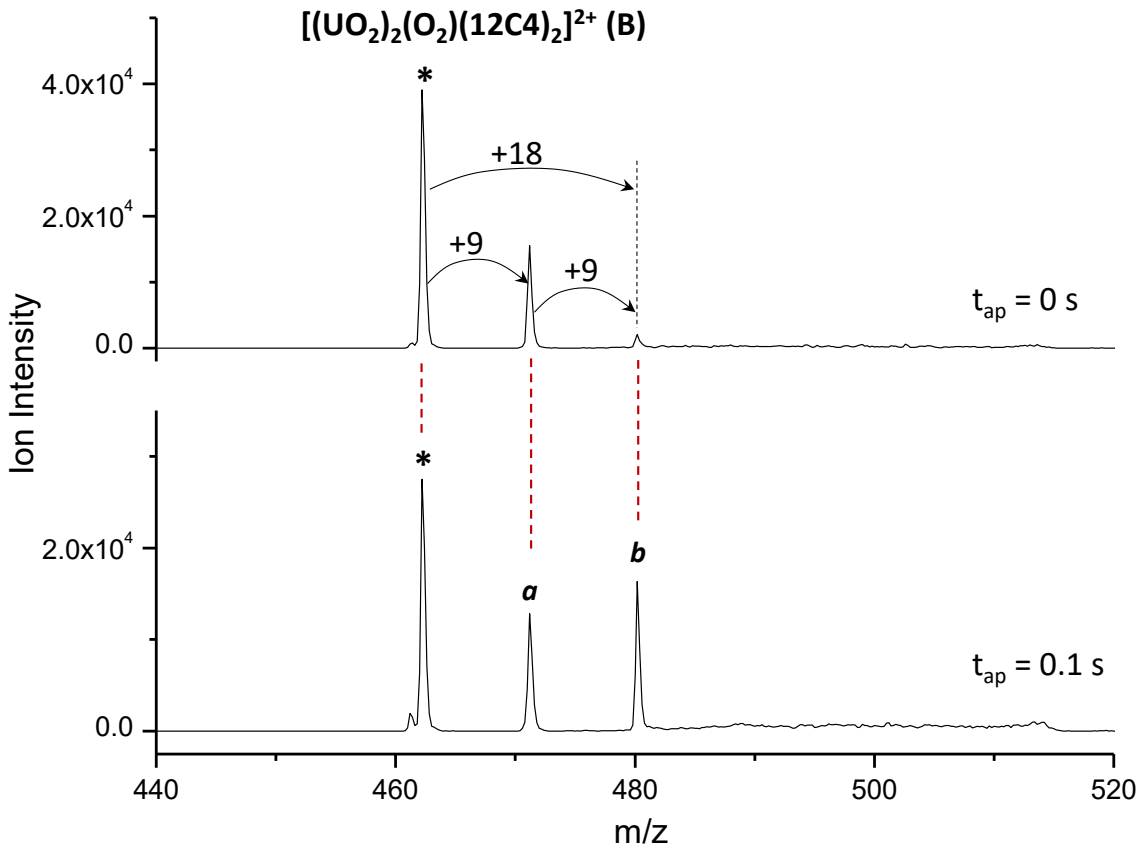

Figure 3. Mass spectra acquired for isolated ions at 462 m/z (marked with asterisk), which corresponds to **B**, after supplemental applied reaction times of 0 s (top) and 0.1 s (bottom). Addition of background H_2O is indicated by $\Delta(m/z) = +9$ for $z = +2$, and $\Delta(m/z) = +18$ for $z = +1$. Product peaks ***a*** and ***b*** are discussed in the text.

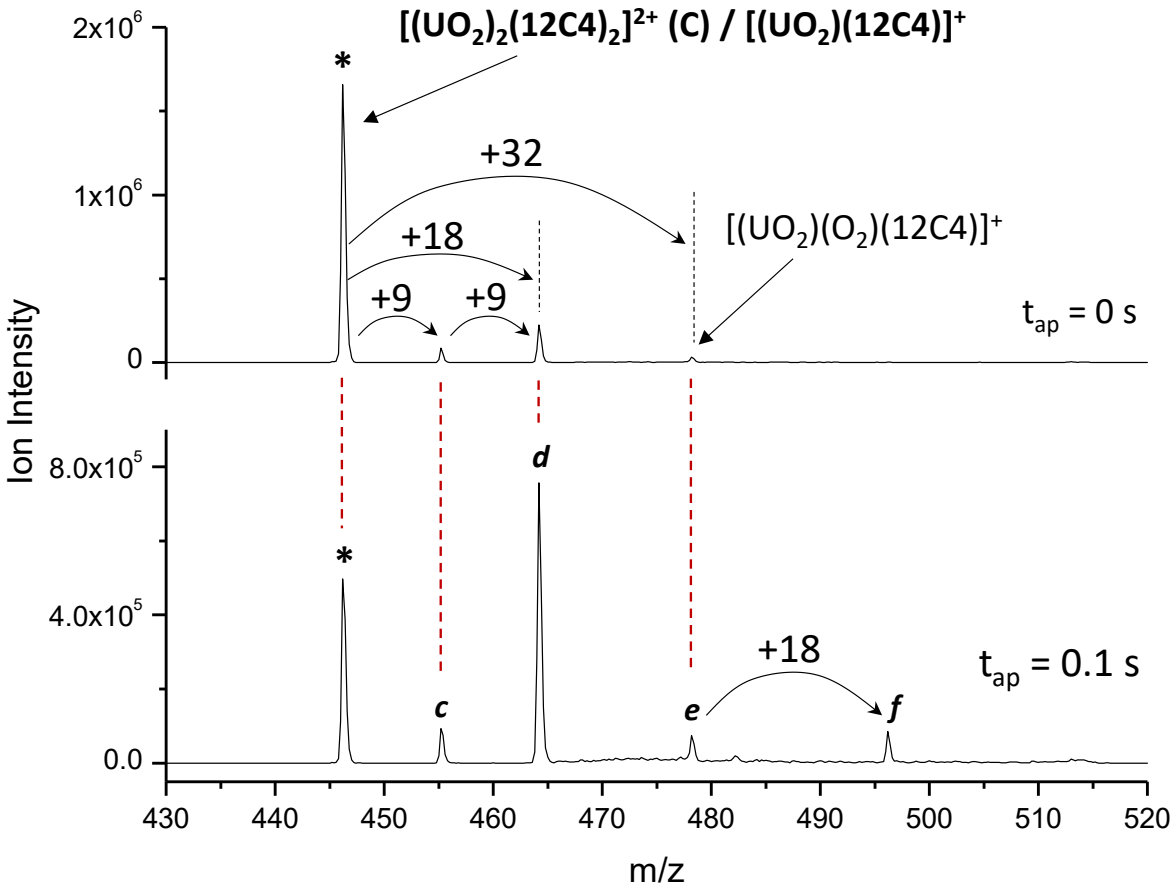

Figure 4. Mass spectra acquired for isolated ions at 446 m/z (marked with asterisk), after applied reaction times of 0 s (top) and 0.1 s (bottom). 446 m/z corresponds to monopositive $[(UO_2)(12C4)]^+$ and/or dipositive $[(UO_2)_2(12C4)_2]^{2+}$ (**C**) Addition of background H_2O is indicated by $\Delta(m/z) = +9$ for $z = +2$ and $\Delta(m/z) = +18$ for $z = +1$. Addition of O_2 is indicated by $\Delta(m/z) = +32$ for $z = +1$.

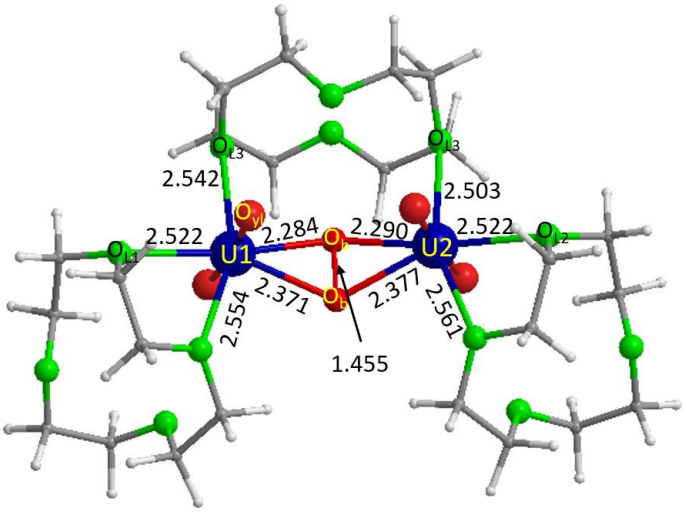

A

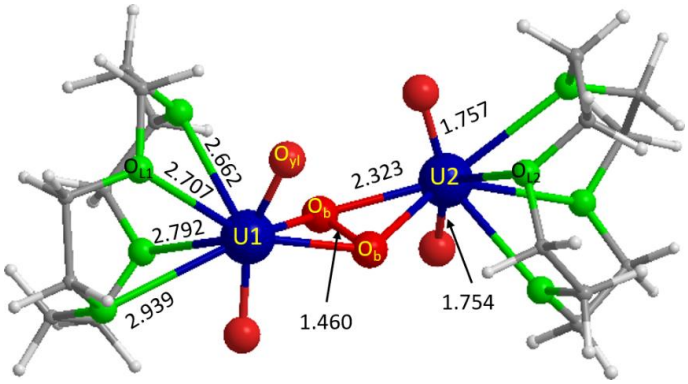

B

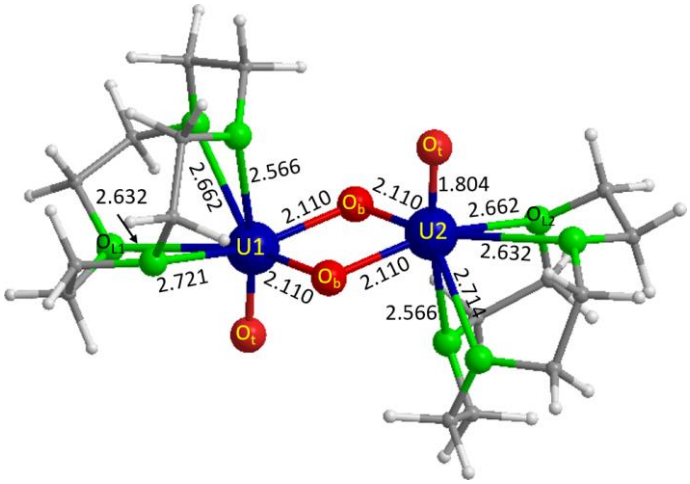

C

Figure 5. Computed structures of GS $[(UO_2)_2(O)_2(12C4)_3]^{2+}$ (**A**), $[(UO_2)_2(O)_2(12C4)_2]^{2+}$ (**B**), and $[(UO_2)_2(12C4)_2]^{2+}$ (**C**). Bond distances are in Å. The O_L in 12C4 are green; other O are red.

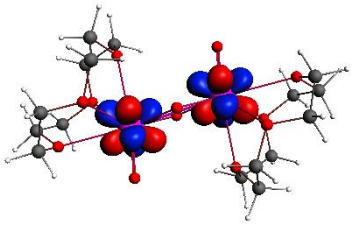

HS-**C**-SOMO

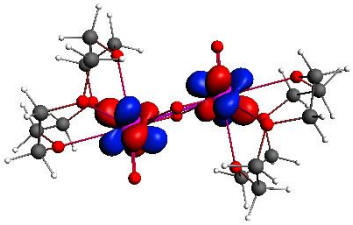

HS-**C** -SOMO-1

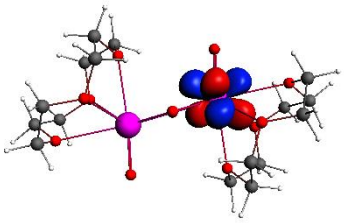

BS-**C**-HOMO-α

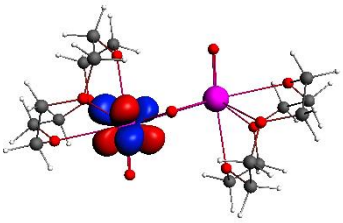

BS-**C**-HOMO-β

Figure 6. Iso-surfaces of frontier MOs of **C** with triplet and broken-symmetry singlet multiplicities at PBE/TZ2P level.

Table of Contents

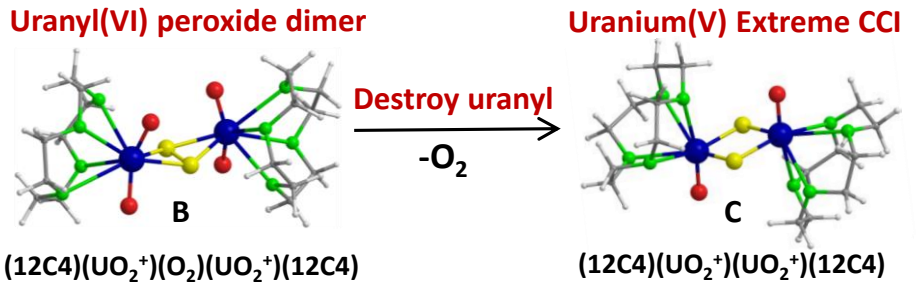

Terminal 12-Crown-4 ether ligands, "12C4", support gas-phase peroxide-bridged uranyl(VI) dimer **B**. Elimination of O_2 from **B** results in destruction of the uranyl O_{yl}=U=O_{yl} moieties concomitant with reduction to U(V), yielding **C** in which two U=O units are linked by two bridging O atoms. Because **C** corresponds to association of two ligated UO_2^+ moieties, it corresponds to a formal "cation-cation" interaction in which the uranyl bonding motif has been practically demolished.